Chapter 2
Theoretical Background

Abstract The theoretical background on photovoltaic (PV) device operation is reviewed. The principle of light absorption in direct and indirect semiconductors, and the use of a p–n and p–i–n devices are explained. Basic performance parameters and one-diode model parameters of solar cells are introduced and explained together with intrinsic and extrinsic loss mechanisms. Extrinsic losses originating from the spatial dimensions of the devices are systematically presented. General recombination processes are reviewed with an emphasis on radiative recombinations, which are the source of luminescence. A distinction is made between a photo- and electroluminescence image based on the type of luminescence excitation. Finally, a summary of the reciprocity relation between PV quantum efficiency and electroluminescence is given.

Keywords Photovoltaics · Thin-film · Operation · Luminescence · Reciprocity relation

2.1 Photovoltaic Device Operation and Performance Parameters

Photovoltaic (PV) devices convert solar energy directly into electrical energy. Solar energy is described as either a spectrum of electromagnetic radiation or a flux of photons. A photon is an elementary particle without mass but with finite energy that corresponds to the frequency or wavelength of the electromagnetic radiation. A correlation between the photon energy (E_{ph}) and wavelength (λ) in vacuum is described by the following equation:

$$E_{ph} = h \cdot \nu = \frac{h \cdot c}{\lambda} \tag{2.1}$$

where h is the Planck's constant, ν is the frequency and c is the speed of light in vacuum. The photons emitted by the sun have different energies; their distribution

M. Bokalič and M. Topič, *Spatially Resolved Characterization in Thin-Film Photovoltaics*, SpringerBriefs in Electrical and Computer Engineering,
DOI 10.1007/978-3-319-14651-5_2

along the energy axis is called the solar radiation spectrum. Solar spectra are standardised to the amount of the Earth's atmosphere they pass through e.g. an air mass (AM) of 0 in space above the atmosphere and AM of 1.5 on the Earth's surface at a 48.2° solar zenith angle. In terrestrial PV the 1,000 W/m^2 AM1.5 spectrum is used as a standard test condition (STC). For certain theoretical calculations, the solar spectrum has also been approximated by a spectrum of a black body at 6,000 K.

The majority of solar cells exploit semiconductor materials to convert light into electricity. A semiconductor is described by its valence and conduction energy bands i.e. a group of energy levels, which electrons may occupy, and a gap in between with no available energy levels called the bandgap. In thermal equilibrium at a 0 K, all the energy levels in the valence band are occupied by electrons while all energy levels in the conduction band remain unoccupied. Energy level occupancy is usually described by the Fermi-Dirac distribution [1]. The exceptions are the active layers in organic and dye-sensitised solar cells, where light interacts with either the organic or dye molecules. Here, the distinct energy levels are described as the highest occupied molecular orbital (HOMO) and lowest unoccupied molecular orbital (LUMO), and the difference between the two may be considered as the bandgap.

Only photons with energies higher than the bandgap can be absorbed in the perfectly pure semiconductor by exciting an electron from the valence to the conduction band, while simultaneously conserving total energy and momentum. Two types of semiconductors are distinguished with regards to the shape of the valence and conduction band in the energy–momentum diagram. In a direct semiconductor, the maximum energy of the valence band and the minimum energy of the conductance band are located at the same momentum, which is not the case in an indirect semiconductor. Light absorption in a direct semiconductor occurs when the photon interacts with only an electron from the valence band. Light absorption in an indirect semiconductor requires a phonon (i.e. a quantum of thermal energy with considerable momentum, which is discernible as a crystal lattice vibration) assisted transition, where a phonon provides or consumes the difference in momentum. Conditions for phonon assisted absorption are much less likely satisfied than for direct absorption. Different absorption mechanisms have a direct impact on PV devices. Direct semiconductors e.g. gallium arsenide, cadmium telluride, and CIGS, are good light absorbers making them ideal for thin-film (TF) PV devices with an absorber layer thickness in the order of μm. They exhibit good absorption for all photons with energies higher than the bandgap and form a sharp absorption edge at the bandgap energy. Indirect semiconductors e.g. crystalline silicon are poorer light absorbers and require a much thicker absorber layer (hundreds of μm). They exhibit good absorption for photons with energy considerably higher than the bandgap and their absorption gradually falls as the photons' energy is decreased towards the bandgap energy. Following the Lambert-Beer law, absorption decreases exponentially with depth where the absorption coefficient (α) is defined by the material properties and is wavelength dependent. The absorption of a photon that results in a free electron in the conduction band and a hole in the valence band

is called a charge carrier generation. The generation rate profile corresponds to the incremental absorption profile. To increase the amount of absorbed light various light management and light trapping techniques can be used [2].

Once the charge carriers are generated, they must be physically separated and need to reach the electrical contacts of the opposite polarity; photogenerated electrons towards the (−) contact and holes towards the (+) contact. Charge carrier collection at the contacts must take place prior to their recombination otherwise their energy is lost. In high quality absorbers the charge carrier lifetime or diffusion length is much higher and the diffusion provides sufficient initial charge carrier separation in the bulk region, enabling the use of a p-n structure with a shallow space charge region (SCR), where a built-in electric field ($\vec{E}$) accelerates the photogenerated carriers towards the contacts (Fig. 2.1a). In materials of lower electronic quality like amorphous semiconductors the charge carrier lifetime is short and separation needs to be assisted by a built-in electric field in the SCR that extends across the whole structure. This is achieved by the use of a p-i-n structure (Fig. 2.1b).

After successful separation, charge carriers must be transported via the conductive layers and wires to the electrical terminals of the PV device, where they are available as electrical energy to an external load.

Concentration of separated charge carriers at the opposite contacts of an illuminated solar cell in open-circuit mode creates a voltage difference known as an open-circuit voltage (V_{OC}). If the contacts are shorted, the voltage drops to zero and a short-circuit current (I_{SC}) starts to flow. When a load with a certain resistance is connected, voltage and current are somewhere between 0 and V_{OC}, and 0 and I_{SC}, respectively. If the load resistance is varied from 0 to infinity the *I-V* characteristic of the device (from I_{SC} to V_{OC}) is obtained (Fig. 2.2b). A point where the maximum power (P_{MPP}) is extracted from the cell is called the maximum power point (MPP). The P_{MPP} is never equal to the product of I_{SC} and V_{OC}, but is reduced primarily by the nature of the p–n junction described by the Shockley diode law, as well as by finite serial resistances R_s and parasitic shunt resistances R_{sh}. The amount of non-ideality is described by the fill factor *FF*:

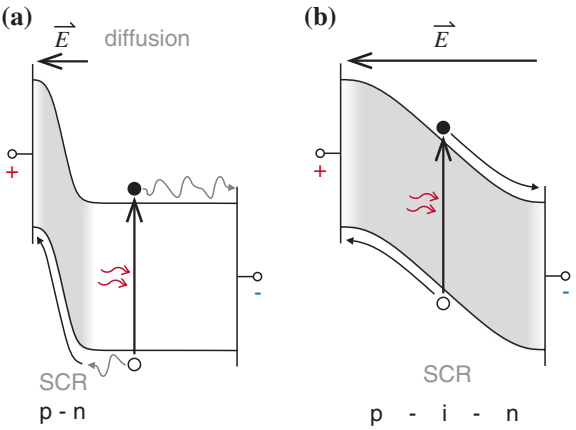

Fig. 2.1 Device structures with charge transport mechanisms: **a** p–n junction, **b** p–i–n junction

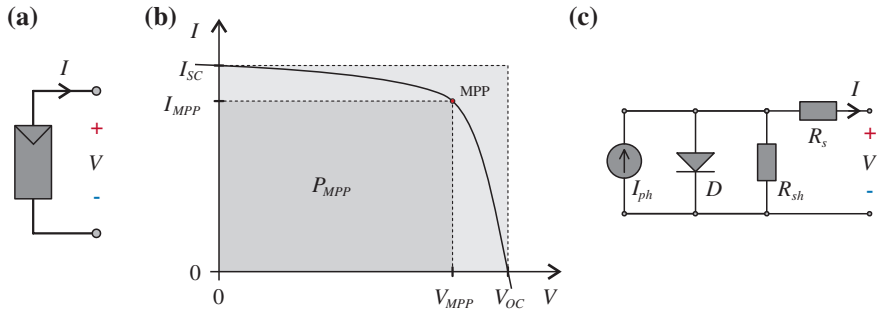

Fig. 2.2 Solar cell representation: **a** a symbol of a solar cell, **b** An *I-V* curve of a solar cell, **c** A one-diode model of a solar cell

$$FF = \frac{P_{MPP}}{I_{SC} \cdot V_{OC}} \tag{2.2}$$

The conversion efficiency η of the solar cell is measured under STC (1,000 W/m^2, AM1.5, 25 °C) and defined as the ratio between the maximum output power and incident solar power P_{in}:

$$\eta = \frac{P_{MPP}}{P_{in}} \tag{2.3}$$

The main solar cell performance parameters under STC are I_{SC}, V_{OC}, P_{MPP}, FF, and η, whereas the whole *I-V* characteristic can be usually described by either a one- or two-diode model [3].

The one diode model of a solar cell (Fig. 2.2c) consists of a photocurrent source (I_{ph}), a diode described by the Shockley diode law (dark saturation current I_0, ideality factor n), and a shunt resistance (R_{sh}) connected in parallel and additionally a series resistance (R_s) connected in series. A one-diode model of a solar cell considering the orientation in Fig. 2.2c is described by the following:

$$I = I_{ph} - I_0 \cdot \left(e^{\frac{q(V+I \cdot R_s)}{n \cdot k \cdot T}} - 1 \right) - \frac{V + I \cdot R_s}{R_{sh}} \tag{2.4}$$

where k is the Boltzmann's constant and T is the cell temperature.

In the *I-V* characteristic of a solar cell the y-axis displaying the absolute current I is area-dependent. To ease the comparison between cells of different areas, a *J-V* characteristic is often used, where I is normalised by the area of the cell to the current density J. Equation (2.4) can be rewritten by changing I to J, and R_s and R_{sh} to r_s and r_{sh} as resistances per area $\left[\Omega / cm^2\right]$.

Photovoltaic devices are energy conversion devices where the energy loss present at the conversion may be distinguished between intrinsic and extrinsic losses. Intrinsic losses are unavoidable even in an idealised solar cell [4]:

- photons with energies lower than the bandgap are not absorbed—*below E_G loss*,
- electron-hole pairs created by photons with energies higher than the bandgap lose all excess energy above the energy of the bandgap due to thermalisation—*thermalisation loss*,
- and other losses imposed by thermodynamic processes and geometries—*emission loss*, *Carnot loss*, and *Boltzman loss* [4].

Extrinsic losses, although theoretically avoidable, are always present in real devices and often a consequence of device topology:

- reflectance from top layers and absorption in transparent layers above the active layers—*optical loss*,
- contact shadowing or inactive areas (e.g. due to monolithic contacts) reduce the active area—*inactive area loss*,
- voltage drop due to series resistance of the contacting layers shifts the operating points of the different device segments—*maximum power point mismatch loss*,
- resistance of electrical contacts causes Joule power dissipation—*series resistance loss*,
- defects in the active layers and manufacturing defects enable parasitic recombination and cause shunts—*shunt resistance loss*.

The theoretical efficiency limits of single junction solar cells calculated by different authors only consider intrinsic losses and result in a 30 % maximum for an absorber with an $E_G = 1.1$ eV [5] and a 32.5 % for an absorber with an $E_G = 1.31$ eV [4] both at 1,000 W/m^2 illumination with black body spectrum at 6,000 K, and a 33.5 % maximum for an absorber with an $E_G = 1.42$ eV at 1,000 W/m^2 illumination with an AM1.5 spectrum [6]. Discrepancies between these results arise from different interpretations of loss mechanisms and different input data, primarily the solar spectrum and its discretisation. A comparison of the theoretical efficiency limits to achieved record efficiencies reveals a difference in absolute efficiency of 10–20 % for TF PV. This difference is due to extrinsic losses, and while some are caused by material properties and are homogeneously distributed across the whole area of the TF PV device, others are caused by localised imperfections, resistance of electrical contacts and the spatial design of the device. It is this latter group of extrinsic losses that can only be precisely characterised using spatially resolved characterisation techniques.

Inhomogeneous extrinsic losses may be distinguished by their influence on neighbouring areas. For example the series resistance of electrical contacts or a poor vertical contact between the layers, reduce the performance of the affected areas only and may be called *neutral*. Others including thinning of the active layer or a highly active recombination centre usually form a shunt that can reduce the performance of the neighbouring areas and may be called *lossy*.

Every inhomogeneity, neutral or lossy, causes a shift in the operating point of the device segment away from the MPP (Fig. 2.3). The energy loss due to a MPP

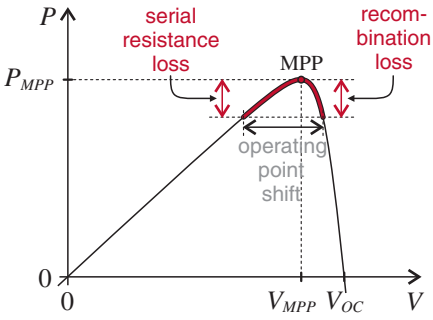

Fig. 2.3 A *P–V* curve of a solar cell illustrating extrinsic losses from maximum power point mismatch

mismatch is lost either as a Joule power dissipation on serial resistances when the device segment's voltage is reduced (marked as serial resistance loss in Fig. 2.3) or as a Joule power dissipation by non-radiative recombinations and a radiation emission by radiative recombinations when the device segment's voltage is increased (marked as recombination loss in Fig. 2.3).

2.2 Luminescence

Luminescence in semiconductors is a consequence of radiative recombinations i.e., annihilation of free electrons and holes in pairs resulting in photon emission, which occur when excess free charge carriers are present within a semiconductor in a PV device. Excess free charge carriers generated by excitation with illumination result in photoluminescence (PL), whereas electrically generated charge carriers result in electroluminescence (EL). Luminescence radiation may be acquired by

(a) a digital camera with an appropriate sensitivity in the anticipated wavelength range to provide spatial information,
(b) a highly sensitive spectrometer to provide spectral information averaged over the measured area, or
(c) a hyperspectral imager to provide spatial and spectral information combined.

Spatial EL is used in research and development (R&D) to detect conversion efficiency inhomogeneities [7, 8] and, supported by simulations, also to investigate their effects on performance. In manufacturing, spatial EL is used for quality control for detecting invisible defects [9, 10]. Spatial PL is used in R&D for investigating semiconductor bulk, surface or junction quality and has recently emerged in industry as an in situ contactless method for early defect detection in crystalline-silicon solar cell production starting with inspection of casted silicon blocks, bricks and wafers [11]. Spectral PL and EL are being intensively developed and are used only in R&D for investigating the origin of radiative recombinations [12–15]. Hyperspectral luminescence imaging is an emerging technique where the main obstacle is low luminescence intensity, nevertheless it has been successfully used for silicon, GaAs, and CIGS PV devices [16–19].

Recombination occurs when a free electron occupies the position of a hole and the energy difference is released in the form of either a photon (radiative recombination), phonons (non-radiative recombination), or a combination of both. When an emission of a photon is present, the recombination is called radiative. Radiative recombinations are inevitable and represent an intrinsic loss, accounted for in the *Boltzman loss* [4]. In an ideal excited semiconductor there would only be radiative band to band recombinations (and non-radiative Auger recombinations), however in actual semiconductors the majority of the recombinations is non-radiative due to defects that cause discrete or distributed energy levels within the bandgap (usually referred to as mid-gap states). Non-radiative recombinations are avoidable in theory and represent an extrinsic loss accounted for in the *shunt resistance loss* [4].

There are several possible types of radiative recombinations: conduction band to valence band, donor to acceptor pair, conduction band to acceptor, donor to valence band, free and bound exciton radiative recombination, and even radiative recombinations through midgap-defects [20, 21]. In reality, a variety of radiative recombinations occur simultaneously and their distribution along the energy axis, i.e. the luminescent spectrum, reveals their type [22]. Because energy level occupancy is dependent on temperature not all types of radiative recombinations occur at the same temperature, hence temperature dependent measurements are used to isolate different types of recombinations [13]. Luminescent spectra at different temperatures contain important information about the material structure of PV devices, their quality, and the electrical processes taking place within.

Alternatively, energy level occupancy and luminescence intensity is dependent on the applied local voltage, which differs across the device due to extrinsic losses. This dependency may be exploited to obtain information about the spatial distribution of the local junction voltage that leads to conversion efficiency. A correlation between luminescence intensity and local conversion efficiency is given in the reciprocity relation.

2.3 Reciprocity Relation

The theoretical limit of efficiency for single junction solar cells first calculated by Shockley and Queisser [5] was based on the principle of detailed balance. The same principle has been used by Rau to derive the reciprocity relation between PV quantum efficiency and electroluminescence emission of solar cells [23]. A summary of this relation is presented herein due to its key importance for interpreting luminescent images.

2.3.1 Thermal Equilibrium

In thermal equilibrium (Fig. 2.4), a solar cell is exposed to radiation from its surroundings, which can be described as a photon flux density of a black body (Φ_{bb}) with refractive index $n = 1$ and temperature T:

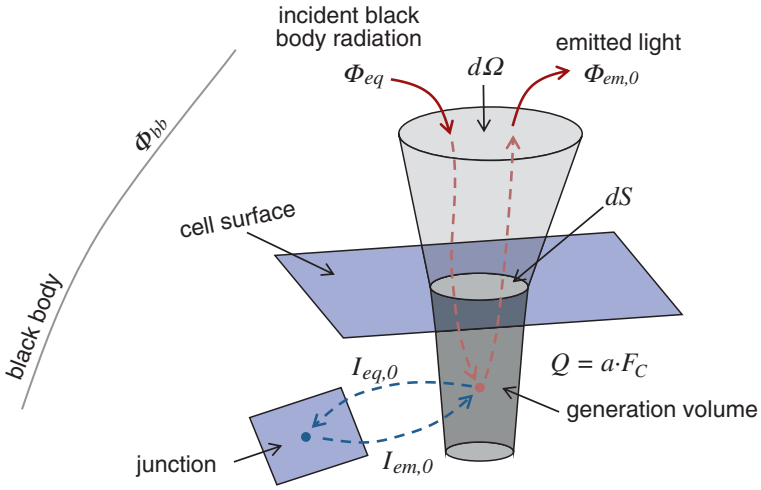

Fig. 2.4 Solar cell in thermal equilibrium exposed to radiation from its surroundings and described as a black body

$$\Phi_{bb}\left(E_{ph},T\right) = \frac{2\cdot E_{ph}^2}{h^2\cdot c^2}\cdot\left(\mathrm{e}^{\frac{E_{ph}}{k\cdot T}}-1\right)^{-1} \tag{2.5}$$

where E_{ph} is the photon energy, h the Planck constant, c the speed of light, and $k\cdot T$ the thermal energy. By assuming $\mathrm{e}^{\frac{E_{ph}}{k\cdot T}} \gg 1$, each part of the cell is irradiated from each incident solid angle Ω of the surroundings by

$$\Phi_{eq}\left(E_{ph},\Omega\right) = \Phi_{bb}\left(E_{ph}\right)\cdot\cos\left(\Omega\right) \approx \frac{2\cdot E_{ph}^2}{h^2\cdot c^2}\cdot\cos\left(\Omega\right)\cdot\mathrm{e}^{-\frac{E_{ph}}{k\cdot T}} \tag{2.6}$$

A part $a\left(\vec{r}_s,\theta,\varphi,E_{ph}\right)$ of the incident photons is absorbed in the cell and a part $F_C\left(\vec{r}_s,\theta,\varphi,E_{ph}\right)$ of the absorbed photons generates free charge carriers. Thus, the total probability that one incident photon will generate a useful charge carrier is

$$Q\left(\vec{r}_s,\theta,\varphi,E_{ph}\right) = a\left(\vec{r}_s,\theta,\varphi,E_{ph}\right)\cdot F_C\left(\vec{r}_s,\theta,\varphi,E_{ph}\right) \tag{2.7}$$

where $\vec{r}_s$ is a point on the surface of the cell, θ the zenith and φ the azimuth incident angle that define the incident solid angle Ω ($d\Omega = \sin\theta\ d\theta\ d\varphi$). Integrating all the useful charge carriers through all incident solid angles Ω, all photon energies E_{ph}, and the whole surface S of the cell yields an equilibrium thermal generation current:

$$I_{eq,0} = q\int\limits_{\Omega}\int\limits_{E_{ph}}\int\limits_{S} Q\left(\vec{r}_s,\Omega,E_{ph}\right)\cdot\Phi_{eq}\left(E_{ph},\Omega\right)\ d\Omega\ dE_{ph}\ dS \tag{2.8}$$

This being the thermal equilibrium means that no net current can exist. Therefore the equilibrium thermal generation current is counterbalanced by a current injection, i.e. emission current in thermal equilibrium, in the opposite direction:

$$I_{em,0} = I_{eq,0} \tag{2.9}$$

A consequence of the current injection is the emission of radiation out of the cell $\Phi_{em,0}$, which is equal to the incident radiation Φ_{eq} and fulfils the detailed balance principle in the equilibrium.

Expressing the average probability of charge carrier generation from Eq. (2.8) and using emission quantities yields the factor that corresponds to the external quantum efficiency (*EQE*) of the solar cell is expressed as:

$$Q = \frac{\frac{I_{em,0}}{q}}{\Phi_{em,0}} = EQE \tag{2.10}$$

Under conditions of Shockley Queisser maximum efficiency, the external quantum efficiency becomes discrete. For photon energies smaller than the bandgap $E_{ph} < E_g$ the *EQE* is zero, for photon energies larger than or equal to the bandgap $E_{ph} \geq E_g$ the *EQE* is unity.

2.3.2 Non-equilibrium

Although the *EQE* can be extracted from equations in thermal equilibrium, none of the unknown quantities in Eq. (2.10) can actually be measured because they are counterbalanced by their opposite quantities on the microscopic level as implied by the detailed balance principle. To measure these quantities the cell must be excited by an external energy source. There are two ways of unbalancing a solar cell that result in different methods.

Electrical excitation by applying current or voltage to the cell results in **electroluminescence** (EL) and causes additional current to flow through the device as shown in Fig. 2.5a. This current is added to the thermal equilibrium current injection $I_{em,0}$ in an exponential manner with respect to the applied voltage as implied by the Shockley's diode law. Net current through the cell I_{em} is the sum of the injection current and the thermal equilibrium thermal generation current $I_{eq,0}$, which is equal to the thermal equilibrium current injection $I_{em,0}$:

$$I_{em} = I_{em,0} \cdot \mathrm{e}^{\frac{q \cdot V}{k \cdot T}} - I_{eq,0} = I_{em,0} \cdot \left(\mathrm{e}^{\frac{q \cdot V}{k \cdot T}} - 1\right) \tag{2.11}$$

This net flow of electrons causes additional electroluminescence photon emission from the cell:

$$\Phi_{EL}\left(\vec{r}_s, \theta, \varphi, E_{ph}\right) = Q\left(\vec{r}_s, \theta, \varphi, E_{ph}\right) \cdot \Phi_{em,0} \cdot \left(\mathrm{e}^{\frac{q \cdot V}{k \cdot T}} - 1\right) \tag{2.12}$$

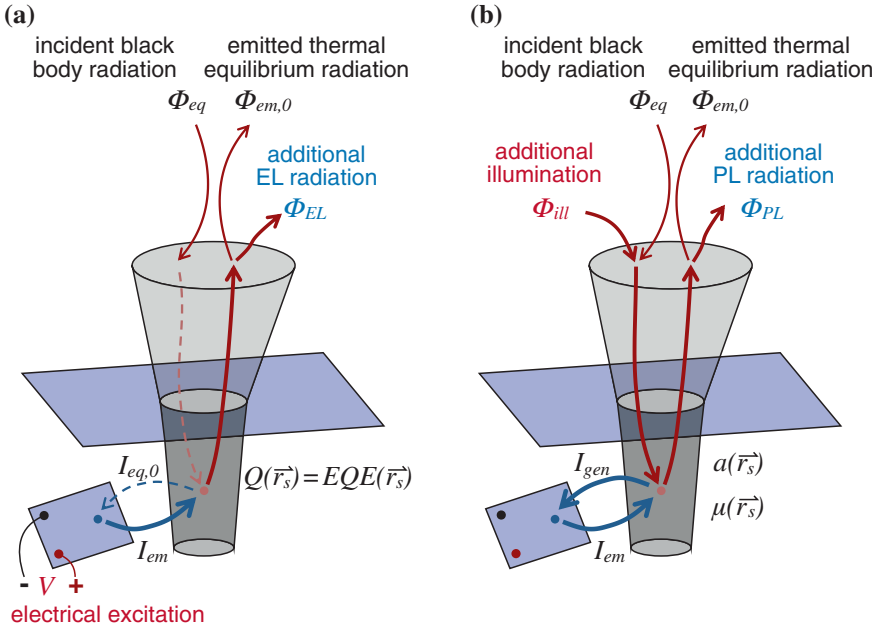

Fig. 2.5 Solar cell in non-equilibrium unbalanced by: **a** electrical excitation—electroluminescence, **b** additional illumination—photoluminescence

Injection current (I_{em}) is known and additional electroluminescence photon emission (Φ_{EL}) can now be measured, and since $Q\left(\vec{r}_s, \theta, \varphi, E_{ph}\right)$ equals $EQE\left(\vec{r}_s, \theta, \varphi, E_{ph}\right)$ (Eq. (2.10)) the extraction of *EQE* is feasible from EL measurements.

Light excitation by exposing a cell to additional illumination (Φ_{ill}) results in **photoluminescence** (PL), (Fig. 2.5b) and again causes additional current to be generated as implied by Eq. (2.8):

$$I_{gen} = q \int_{\Omega} \int_{E_{ph}} \int_{S} Q\left(\vec{r}_s, \theta, \varphi, E_{ph}\right) \cdot \Phi_{ill} \cdot \left(E_{ph}, \Omega\right) \, d\Omega \, dE_{ph} \, dS \tag{2.13}$$

If a cell was electrically connected to the load it would have been in a generator regime and a part of I_{gen} would have been spent on the load; however when a cell is kept in the open-circuit (Fig. 2.5b) charge carriers are still generated, but have nowhere to go, except to recombine and cause additional PL emission (Φ_{PL}), which is found to be proportional to the splitting of the quasi-Fermi levels (μ):

$$\Phi_{PL}\left(\vec{r}_s, \theta, \varphi, E_{ph}\right) \approx a\left(\vec{r}_s, \theta, \varphi, E_{ph}\right) \cdot \Phi_{ill} \cdot \left(\mathrm{e}^{\frac{\mu}{k \cdot T}} - 1\right) \tag{2.14}$$

Comparison of Eq. (2.14) with (2.12) shows the similarities between EL and PL. Splitting of the quasi-Fermi levels μ takes the role of the applied voltage V, and the absorption $a\left(\vec{r}_s, \theta, \varphi, E_{ph}\right)$ takes the role of the probability of the charge

carrier generation $Q(\vec{r}_s, \theta, \varphi, E_{ph})$, which corresponds to the external quantum efficiency $EQE(\vec{r}_s, \theta, \varphi, E_{ph})$. Despite the similarities, *EQE* does not equal absorption *a*, since the former is also influenced by serial resistance.

Results obtained by EL include all factors that influence a solar cell's performance. This includes electrical contacts and serial resistance and provides the information about spatially resolved *EQE*. PL might seem inferior to EL because its results do not include influence of electrical contacts and serial resistance; however it offers other advantages. Because no electrical contacts are needed for PL, it may be used in early production stages when electrical contacts are not yet made. Additionally, for excitation during PL measurements a monochromatic light may be used. The wavelength of this light defines at which depth it will be absorbed, and for direct semiconductors with fast radiative recombination this depth defines the approximate source of the PL signal and provides information about a certain layer up to a certain depth in the cell.

2.3.3 Usage and Validity

Detailed balance and reciprocity relations have been derived between several processes occurring in solar cells [24] and have also been extended to excitonic and bulk heterojunction cells [25]. The reciprocity theory was the theoretical foundation for EL investigation of crystalline silicon [26], CIGS [22], and GaInP/GaInAs/Ge based multijunction PV devices [27]. Deviations from reciprocity theory were observed for microcrystalline silicon [15] and amorphous silicon [28] PV devices, where tail-to-tail and band-to-midgap-defects radiative recombinations become dominant and violate the conditions for reciprocity relation [23]. Lately, the reciprocity relation has been extended to the superposition of electroluminescence and photoluminescence [29] and between various other important quantities in solar cells [30].

2.4 Summary

A brief theoretical background of solar cell operation was given in this chapter. Light is absorbed in different types of absorbers and can be transformed to useful electrical energy. Performance parameters are extracted from the *I-V* characteristic of the solar cell. The incident solar energy is lost mainly due to unavoidable intrinsic losses, but also to avoidable extrinsic losses, which are often caused by inhomogeneities. To discover inhomogeneous extrinsic losses, spatially resolved characterisation methods must be used. These methods often rely on luminescence, which is a consequence of radiative recombinations. Luminescence phenomenon in solar cells is explained and theoretically linked to the performance parameters of solar cells via reciprocity relations.

References

1. Pierret RF (2003) Advanced semiconductor fundamentals. Prentice Hall/Pearson Education, Upper Saddle River
2. Krč J, Topič M (2013) Optical modeling and simulation of thin-film photovoltaic devices. CRC Press, Boca Raton
3. Green MA (1982) Solar cells: operating principles, technology, and system applications. Prentice-Hall, Englewood Cliffs
4. Hirst LC, Ekins-Daukes NJ (2011) Fundamental losses in solar cells. Prog Photovolt Res Appl 19:286–293. doi:10.1002/pip.1024
5. Shockley W, Queisser HJ (1961) Detailed balance limit of efficiency of p-n junction solar cells. J Appl Phys 32:510–519. doi:10.1063/1.1736034
6. Miller OD, Yablonovitch E, Kurtz SR (2012) Strong internal and external luminescence as solar cells approach the shockley-queisser limit. IEEE J Photovolt 2:303–311. doi:10.1109/JPHOTOV.2012.2198434
7. Fuyuki T, Kondo H, Yamazaki T, Takahashi Y, Uraoka Y (2005) Photographic surveying of minority carrier diffusion length in polycrystalline silicon solar cells by electroluminescence. Appl Phys Lett 86:262108–262108-3. doi:10.1063/1.1978979
8. Haunschild J, Glatthaar M, Kasemann M, Rein S, Weber ER (2009) Fast series resistance imaging for silicon solar cells using electroluminescence. Phys Status Solidi Rapid Res Lett 3:227–229. doi:10.1002/pssr.200903175
9. Bokalič M, Černivec G, Demolliens A, Revel J, Topič M, Poličnik M, Merc U (2010) Electroluminescence findings and IR LED I-V curve measurement in (wafer-based) solar cell module production. In: 25th European photovoltaic solar energy conference and 5th world conference on photovoltaic energy conversion. WIP-Renewable Energies, Valencia, Spain, pp 4184–4188
10. Chunduri SK (2011) No place to hide-market survey on luminescence imaging systems and cameras. Photon Int 1:158
11. Michl B, Padilla M, Geisemeyer I, Haag ST, Schindler F, Schubert MC, Warta W (2014) Imaging techniques for quantitative silicon material and solar cell analysis. IEEE J Photovolt 4:1502–1510. doi:10.1109/JPHOTOV.2014.2358795
12. Kirchartz T, Helbig A, Rau U (2008) Note on the interpretation of electroluminescence images using their spectral information. Sol Energ Mat Sol Cells 92:1621–1627. doi:10.1016/j.solmat.2008.07.013
13. Kirchartz T, Rau U, Kurth M, Mattheis J, Werner JH (2007) Comparative study of electroluminescence from Cu(In, Ga)Se_2 and Si solar cells. Thin Solid Films 515:6238–6242. doi:10.1016/j.tsf.2006.12.105
14. Trupke T, Würfel P, Uhlendorf I, Lauermann I (1999) Electroluminescence of the dye-sensitized solar cell. J Phys Chem B 103:1905–1910. doi:10.1021/jp982555a
15. Müller TCM, Pieters BE, Kirchartz T, Carius R, Rau U (2012) Modelling of photo- and electroluminescence of hydrogenated microcrystalline silicon solar cells. Phys Status Solidi C 9:1963–1967. doi:10.1002/pssc.201200428
16. Li Q, Wang W, Ma C, Zhu Z (2010) Detection of physical defects in solar cells by hyperspectral imaging technology. Opt Laser Technol 42:1010–1013. doi:10.1016/j.optlastec.2010.01.022
17. Peloso MP, Lew JS, Hoex B, Aberle AG (2012) Line-imaging spectroscopy for characterisation of silicon wafer solar cells. Energy Procedia 15:171–178. doi:10.1016/j.egypro.2012.02.020
18. Delamarre A, Lombez L, Guillemoles JF (2012) Characterization of solar cells using electroluminescence and photoluminescence hyperspectral images. J Photon Energy 2:027004. doi:10.1117/1.JPE.2.027004
19. Delamarre A (2013) Mapping solar cell parameters using hyperspectral imaging. SPIE newsroom. doi:10.1117/2.1201304.004777

20. Abou-Ras D, Kirchartz T, Rau U (2011) Advanced characterization techniques for thin film solar cells. Wiley-VCH Verlag GmbH & Co. KGaA, Weinheim
21. Müller TCM, Pieters BE, Kirchartz T, Carius R, Rau U (2014) Effect of localized states on the reciprocity between quantum efficiency and electroluminescence in Cu(In, Ga)Se2 and Si thin-film solar cells. Sol Energ Mat Sol Cells 126:95–130. doi:10.1016/j.solmat.2014.04.018
22. Kirchartz T, Rau U (2007) Electroluminescence analysis of high efficiency Cu(In, Ga)Se_2 solar cells. J Appl Phys 102:104510. doi:10.1063/1.2817959
23. Rau U (2007) Reciprocity relation between photovoltaic quantum efficiency and electroluminescent emission of solar cells. Phys Rev B 76:085303. doi:10.1103/PhysRevB.76.085303
24. Kirchartz T, Rau U (2008) Detailed balance and reciprocity in solar cells. Phys Status Solidi A 205:2737–2751. doi:10.1002/pssa.200880458
25. Kirchartz T, Mattheis J, Rau U (2008) Detailed balance theory of excitonic and bulk heterojunction solar cells. Phys Rev B 78:235320. doi:10.1103/PhysRevB.78.235320
26. Kirchartz T, Helbig A, Reetz W, Reuter M, Werner JH, Rau U (2009) Reciprocity between electroluminescence and quantum efficiency used for the characterization of silicon solar cells. Prog Photovolt Res Appl 17:394–402. doi:10.1002/pip.895
27. Kirchartz T, Rau U, Hermle M, Bett AW, Helbig A, Werner JH (2008) Internal voltages in GaInP/GaInAs/Ge multijunction solar cells determined by electroluminescence measurements. Appl Phys Lett 92:123502. doi:10.1063/1.2903101
28. Tran TMH, Pieters BE, Schneemann M, Müller TCM, Gerber A, Kirchartz T, Rau U (2013) Quantitative evaluation method for electroluminescence images of a-Si: H thin-film solar modules. Phys Status Solidi Rapid Res Lett 7:627–630. doi:10.1002/pssr.201308039
29. Rau U (2012) Superposition and reciprocity in the electroluminescence and photoluminescence of solar cells. IEEE J Photovolt 2:169–172. doi:10.1109/JPHOTOV.2011.2179018
30. Wong J, Green MA (2012) From junction to terminal: extended reciprocity relations in solar cell operation. Phys Rev B. doi:10.1103/PhysRevB.85.235205

http://www.springer.com/978-3-319-14650-8

Spatially Resolved Characterization in Thin-Film Photovoltaics

Bokalic, M.; Topic, M.

2015, XIV, 99 p. 57 illus., 39 illus. in color., Softcover
ISBN: 978-3-319-14650-8